

**Resonant dipole-dipole interactions in electromagnetically induced transparency**H. H. Jen <sup>1,2,\*</sup>, G.-D. Lin,<sup>3,2</sup> and Y.-C. Chen<sup>1,4,2</sup><sup>1</sup>*Institute of Atomic and Molecular Sciences, Academia Sinica, Taipei 10617, Taiwan*<sup>2</sup>*Physics Division, National Center for Theoretical Sciences, Taipei 10617, Taiwan*<sup>3</sup>*Department of Physics, National Taiwan University, Taipei 10617, Taiwan*<sup>4</sup>*Center for Quantum Technology, Hsinchu 30013, Taiwan*

(Received 29 December 2021; accepted 1 June 2022; published 14 June 2022)

Resonant dipole-dipole interaction (RDDI) emerges in strong light-matter interacting systems, which leads to many fascinating phenomena such as cooperative light scattering and collective radiation. Here, we theoretically investigate the role of RDDI in electromagnetically induced transparency (EIT). The resonant dipole-dipole interactions manifest themselves in the cooperative spontaneous emission of the probe light transition, which give rise a broadened linewidth and associated collective frequency shift. This cooperative linewidth originates from the nonlocal and long-range RDDI, which can be determined by the atomic density, optical depth, and macroscopic length scales of the atomic ensemble. We present the finding that EIT spectroscopy essentially demonstrates all-order multiple scattering of RDDI. Furthermore, we find that the EIT transparency window becomes narrower as the cooperative linewidth increases, which essentially reduces the storage efficiency of slow light as an EIT-based quantum memory application.

DOI: [10.1103/PhysRevA.105.063711](https://doi.org/10.1103/PhysRevA.105.063711)**I. INTRODUCTION**

Electromagnetically induced transparency (EIT) [1–4] is a robust technique to store a light field while preserving its quantum coherence with little dissipation. This facilitates a quantum interface [5] of light and matter with high efficiency and controllability. Due to the dramatic modification of the dispersive properties accompanying the induced transparency, the probe field propagates through the interacting medium with a reduced group velocity [6,7]. Furthermore, the picture of the dark-state polariton [8] can be adopted to describe light-matter dynamics, where light can be stopped and transferred to atomic coherences and then retrieved back to light again by turning off and on the control field. In addition to neutral atoms [3,4,9,10], EIT has been implemented in various platforms including quantum degenerate gases [6,7], Rydberg atoms [11–14], single atoms in a cavity [15,16], embedded Fe nuclei [17], color centers in a diamond [18,19], semiconductor quantum wells [20], and crystals doped with rare-earth ions [21–25].

The conventional EIT theory [3,4] is mainly based on classical electrodynamics with a mean-field treatment of the dipole operators that govern the light-matter interactions [26]. This theory has been extended to investigate a strongly correlated quantum degenerate gas [27], where intriguing quantum many-body effects emerge in EIT spectroscopy when the atoms are coupled to the low-lying Rydberg states [28,29]. On the other hand, even when the atomic ground state is not in a quantum degenerate regime, which is the case for cold atoms in general, the conventional EIT theory neglects a full

account of the effect of resonant dipole-dipole interactions (RDDIs) [30] in the dissipation channels of both probe and control fields. This effect is crucial especially for atoms of a high density or with a large optical depth (OD), which leads to super-radiance [31,32] and other cooperative spontaneous emissions. Therefore the conventional EIT theory has to be extended in this regard to include the essential collective scattering events mediated by the nonlocal and long-range RDDIs.

There has been huge progress in recent experiments which demonstrate the effect of RDDIs in collective radiation. These rescattering emissions between two atoms can enhance the light emission in a dense atomic medium [33] and are responsible for subradiant emissions in neutral atoms [34], plasmonic nanocavities [35], ultracold molecules [36], and metamolecules [37]. The associated collective frequency shifts can also be observed in various two-level atomic systems of embedded Fe nuclei [38], an atomic vapor layer [39], ions [40], and cold atoms [41–44]. However, this evident cooperative phenomenon has been elusive in the EIT platform of a  $\Lambda$ -type atomic configuration as shown in Fig. 1. Only recently has a semiclassical treatment of light-matter interactions been applied in studying EIT properties with comparable probe and control fields [45], where light-mediated interactions can modify the transparency window. Here in this paper, in contrast, we include the RDDI in the conventional EIT theory involving up to single atomic excitation and derive the effective linewidth broadening and frequency shift in EIT transmission. We show that the probe field propagates through a narrowing EIT transmission window when RDDI is significant. This reflects the nonlocal nature of RDDI, which incorporates all pairwise dipole-dipole interactions and could be observable in future EIT measurements.

\*sappyjen@gmail.com

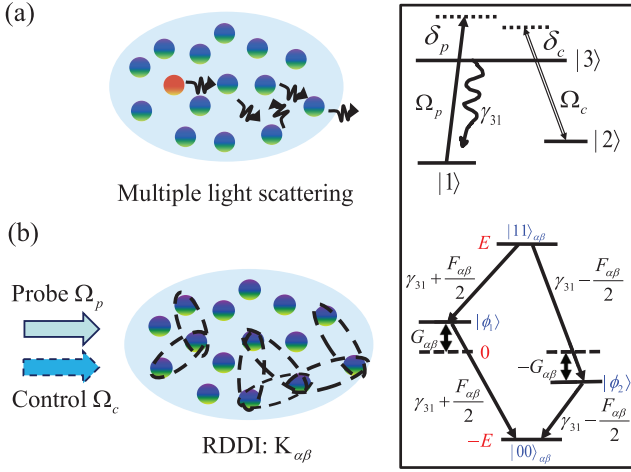


FIG. 1. Schematic plot of multiple scattering of light and the EIT scheme with RDDI. (a) An excited atom emits and scatters light through many rescattering events between atoms before leaving the medium and being observed. (b) A conventional EIT scheme with control field  $\Omega_c$  and probe field  $\Omega_p$  interacting with three-level configurations as shown in the upper inset plot with spontaneous emission decay rate  $\gamma_{31}$ . Probe and control field detunings are denoted as  $\delta_p$  and  $\delta_c$ , respectively. With the effect of pairwise RDDI  $K_{\alpha\beta}$ , which involves a collective decay  $F_{\alpha\beta}$  and frequency shift  $G_{\alpha\beta}$  between all of the other atoms, a level diagram for two atoms is presented in the lower inset plot as a demonstration, where super- and subradiant eigenvalue decay rates  $\gamma_{31} \pm F_{\alpha\beta}/2$  are associated with eigenstates  $|\phi_{1(2)}\rangle = (|01\rangle_{\alpha\beta} \pm |10\rangle_{\alpha\beta})/\sqrt{2}$ , respectively.

The paper is organized as follows. In Sec. II, we consider an EIT scheme in an atomic ensemble, where we obtain the transmission property from the coupled equations with RDDI and their steady-state solutions. We next investigate the linewidth of the probe light transition in Sec. III and present the results of multiple scattering of RDDI in the transmission spectrum in Sec. IV. We also discuss the extension beyond the local field approximation in Sec. V. Finally, we discuss our findings and conclude in Sec. VI. In Appendix A, we obtain Maxwell-Bloch equations with RDDI in the probe field transition, and in Appendix B, we present the steady-state solutions from Maxwell-Bloch equations.

## II. RDDI EFFECT IN EIT

### A. Hamiltonian and Lindblad forms

The effect of RDDI in light propagation is mainly investigated in  $N$  two-level atoms, where a coupled-dipole model along with Maxwell-Bloch equations can describe light-atom dynamics [46]. This treatment is valid when a weak driving field is considered, which effectively takes into account the effects from both RDDI and the propagating light field in the time-evolving atomic coherences. This leads to an effective linewidth broadening and associated frequency shift for the light field transition [44,47,48]. We follow a similar treatment in our EIT setup using  $\Lambda$ -type atoms (as shown in Fig. 1), where a probe field  $\Omega_p$  couples the ground state  $|1\rangle$  to the excited state  $|3\rangle$  while a control field  $\Omega_c$  couples  $|3\rangle$  to the other hyperfine ground state  $|2\rangle$ . The ground-state coherence

is established on absorbing a probe and emitting a control photon, which excites one of  $N$  atoms to  $|2\rangle$  collectively. Therefore a probe photon exchanging with atomic coherence forms a dark-state polariton which propagates through the medium, almost immune to the intrinsic spontaneous emission  $\gamma_{31}$ , and thus keeps its waveform intact inside the medium. Since light couples the atoms collectively, RDDI in the dissipation process should have an effect on EIT spectroscopy, especially for a dense atomic cloud.

For a conventional EIT setup [9], as an example, the system parameters are  $N \sim 5 \times 10^9$  in a cloud size of  $3 \times 3 \times 14 \text{ mm}^3$ , which has an average atomic density of  $\sim 4 \times 10^{10} \text{ cm}^{-3}$ . For a peak density around  $10^{11} \text{ cm}^{-3}$  and considering an interaction volume determined by probe field propagation along the long axis with a cylindrical geometry of  $\pi(0.2)^2 \times 14 \text{ mm}^3$ , we have  $N \sim 1.8 \times 10^8$  with an optical density of  $\sim 400$ . This parameter regime is particularly relevant in conventional EIT experiments as quantum memory applications, where the propagation effect of the probe field becomes essential. In this parameter regime, there is no possible numerical simulation using present computation technology. Therefore we intend to provide an analytical calculation of EIT spectroscopy in a cigar shape of atoms with a relatively large optical density under a moderate atomic density of the order of  $10^{10}$ – $10^{11} \text{ cm}^{-3}$ . In such a long sample of atoms, we note that the Beer-Lambert law for light propagation can be retrieved and sustained, which would otherwise break down in a thin slab geometry of dense atoms [49].

Here, we include and focus on the effect of RDDI in the probe transition and investigate how it modifies the conventional EIT theory. This RDDI should also manifest itself in the control field transition and between two ground states, with respective intrinsic decay rates  $\gamma_{32}$  and  $\gamma_{21}$ . However, a relatively large  $\Omega_c$  and vanishing populations in  $|2\rangle$  and  $|3\rangle$  are legitimate to neglect this effect on  $\gamma_{32}$ , in contrast to the weak  $\Omega_p$ . The ground-state decoherence also involves an inappreciable dipole transition, and therefore the effect of RDDI on  $\gamma_{21}$  should be insignificant compared with that on  $\gamma_{31}$ .

The Hamiltonian for EIT in the interaction picture reads

$$\begin{aligned} \hat{H}_I = & \hbar\delta_p \sum_{\mu=1}^N \hat{\sigma}_{11}^{\mu} + \hbar\delta_c \sum_{\mu=1}^N \hat{\sigma}_{22}^{\mu} \\ & + \sum_{\mu=1}^N \left( -\frac{\hbar\Omega_p}{2} e^{i\mathbf{k}_p \cdot \mathbf{r}_\mu} \hat{\sigma}_{13}^{\mu, \dagger} + \text{H.c.} \right) \\ & + \sum_{\mu=1}^N \left( -\frac{\hbar\Omega_c}{2} e^{i\mathbf{k}_c \cdot \mathbf{r}_\mu} \hat{\sigma}_{23}^{\mu, \dagger} + \text{H.c.} \right), \end{aligned} \quad (1)$$

where the wave vectors of the fields are  $\mathbf{k}_p$  and  $\mathbf{k}_c$  with the Rabi frequencies  $\Omega_p$  and  $\Omega_c$ , respectively, and the atomic dipole operators are  $\hat{\sigma}_{ij}^{\beta} \equiv |i\rangle_{\beta}\langle j|$ ,  $\hat{\sigma}_{ij}^{\beta, \dagger} \equiv \hat{\sigma}_{ji}^{\beta}$ . The detunings are defined as  $\delta_p = \omega_p - \omega_{31}$  and  $\delta_c = \omega_c - \omega_{32}$ , where the central frequencies of light fields are  $\omega_p$ ,  $\omega_c$ , and the atomic transition frequencies are  $\omega_{31}$ ,  $\omega_{32}$ . To account for the RDDI effect in the probe field transition, we use Lindblad forms [50] to fully describe the system dynamics, and the master equation for arbitrary operators  $\hat{Q}$  in the Heisenberg

picture becomes

$$\begin{aligned} \frac{d\hat{Q}}{dt} = & -\frac{i}{\hbar}[\hat{Q}, \hat{H}_I] - i \sum_{\mu \neq \nu}^N [\hat{Q}, G_{\mu\nu} \hat{\sigma}_{31}^{\mu} \hat{\sigma}_{13}^{\nu}] \\ & + \mathcal{L}_p[\hat{Q}] + \mathcal{L}_c[\hat{Q}] + \mathcal{L}_g[\hat{Q}], \end{aligned} \quad (2)$$

where

$$\mathcal{L}_p[\hat{Q}] \equiv - \sum_{\mu, \nu}^N \frac{F_{\mu\nu}}{2} (\hat{\sigma}_{31}^{\mu} \hat{\sigma}_{13}^{\nu} \hat{Q} + \hat{Q} \hat{\sigma}_{31}^{\mu} \hat{\sigma}_{13}^{\nu} - 2\hat{\sigma}_{31}^{\mu} \hat{Q} \hat{\sigma}_{13}^{\nu}), \quad (3)$$

$$\mathcal{L}_c[\hat{Q}] \equiv - \sum_{\mu, \nu}^N \gamma_{32} (\hat{\sigma}_{32}^{\mu} \hat{\sigma}_{23}^{\nu} \hat{Q} + \hat{Q} \hat{\sigma}_{32}^{\mu} \hat{\sigma}_{23}^{\nu} - 2\hat{\sigma}_{32}^{\mu} \hat{Q} \hat{\sigma}_{23}^{\nu}), \quad (4)$$

$$\mathcal{L}_g[\hat{Q}] \equiv - \sum_{\mu, \nu}^N \gamma_{21} (\hat{\sigma}_{21}^{\mu} \hat{\sigma}_{12}^{\nu} \hat{Q} + \hat{Q} \hat{\sigma}_{21}^{\mu} \hat{\sigma}_{12}^{\nu} - 2\hat{\sigma}_{21}^{\mu} \hat{Q} \hat{\sigma}_{12}^{\nu}). \quad (5)$$

The cooperative spontaneous decay rates  $F_{\mu\nu}$  and frequency shifts  $G_{\mu\nu}$  can be expressed as [30]

$$\begin{aligned} F_{\mu\nu}(\xi) \equiv & \frac{3\Gamma}{2} \left\{ [1 - (\hat{d} \cdot \hat{r}_{\mu\nu})^2] \frac{\sin \xi}{\xi} \right. \\ & \left. + [1 - 3(\hat{d} \cdot \hat{r}_{\mu\nu})^2] \left( \frac{\cos \xi}{\xi^2} - \frac{\sin \xi}{\xi^3} \right) \right\}, \end{aligned} \quad (6)$$

$$\begin{aligned} G_{\mu\nu}(\xi) \equiv & \frac{3\Gamma}{4} \left\{ -[1 - (\hat{d} \cdot \hat{r}_{\mu\nu})^2] \frac{\cos \xi}{\xi} \right. \\ & \left. + [1 - 3(\hat{d} \cdot \hat{r}_{\mu\nu})^2] \left( \frac{\sin \xi}{\xi^2} + \frac{\cos \xi}{\xi^3} \right) \right\}, \end{aligned} \quad (7)$$

where  $\Gamma = 2\gamma_{31} \equiv \omega_{31}^3 d^2 / (3\pi \epsilon_0 \hbar c^3)$  is the intrinsic decay rate and  $\hat{d}$  is the dipole orientation with dipole moment  $d$ . The dimensionless scale of mutual separation is  $\xi = |\mathbf{k}_p| r_{\mu\nu}$  with  $r_{\mu\nu} = |\mathbf{r}_{\mu} - \mathbf{r}_{\nu}|$ . The above indicates the long-range nature of dipole-dipole interactions, which is responsible for the cooperative radiation of super-radiance or subradiance. As  $\xi \rightarrow 0$ ,  $F_{\mu\nu}$  approaches  $\Gamma$  while  $G_{\mu\nu}$  becomes divergent, showing an incomplete quantum optical treatment in this limit. For  $\xi \gg 2\pi$  or  $r_{\mu\nu} \gg \lambda$  (transition wavelength), both cooperative decay rates and frequency shifts diminish, which reaches the noninteracting regime of independent atoms.

## B. Maxwell-Bloch equations and the transmission coefficient

From the Maxwell-Bloch equations we obtain in Appendix A, we have truncated the coupled equations at the first-order cumulants [51] or one-body expectation values. This allows self-consistent and dynamically coupled equations, where a hierarchy of many-body correlations are assumed to be insignificant. We define the cross-grained and slow-varying atomic coherence in the probe transition as  $\tilde{\sigma}_{13} = N_z^{-1} \sum_{\beta=1}^{N_z} \hat{\sigma}_{13}^{\beta}(z, t) e^{i\omega_p t - i\mathbf{k}_p \cdot \mathbf{r}_{\beta}}$ , and from Eq. (A5) we obtain

$$\begin{aligned} \frac{d}{d\tau} \tilde{\sigma}_{13} \approx & (i\delta_p - \gamma_{31}) \tilde{\sigma}_{13} + i \frac{\Omega_c}{2} \tilde{\sigma}_{12} + i \frac{\Omega_p}{2} \\ & - \frac{1}{N_z} \sum_{\alpha=1}^{N_z} \sum_{\beta \neq \alpha}^N K_{\alpha\beta} \tilde{\sigma}_{13}^{\beta}, \end{aligned} \quad (8)$$

where  $\tau = t - z/c$  in a copropagating frame, slow-varying atomic operator  $\tilde{\sigma}_{13}^{\beta} \equiv \hat{\sigma}_{13}^{\beta} e^{i\omega_p t - i\mathbf{k}_p \cdot \mathbf{r}_{\beta}}$ , and  $K_{\alpha\beta} \equiv (F_{\alpha\beta} + i2G_{\alpha\beta}) e^{-i\mathbf{k}_p \cdot \mathbf{r}_{\alpha\beta}} / 2$ . In Eq. (8), we have assumed that most of the atoms are in the ground state  $\tilde{\sigma}_{11} \approx 1$ , which is valid in the linear response regime with a weak probe field.  $N_z \equiv N/M$  denotes the number of atoms in  $M$  cross-grained sections along the propagation direction in  $\hat{z}$ , which is introduced as a functional and does not come into play in the continuous limit of field quantization under large  $N$ ,  $N_z$ , and  $M$  [52]. Equation (8) shows the nonlocal ( $r_{\alpha\beta}^{-1}$  in the long range) and linear couplings between atoms throughout the medium via RDDI, in contrast to Rydberg van der Waals interactions ( $\propto r_{\alpha\beta}^{-6}$ ) [12,53] where nonlinear interactions result from two or more Rydberg excitations, and a dipole-blockade sphere can be established due to the large energy shift.

We then solve the steady-state ground-state coherence as shown in Appendix A,

$$\tilde{\sigma}_{12} = \frac{-\Omega_c^*/2}{\delta_2 + i\gamma_{21}} \tilde{\sigma}_{13}, \quad (9)$$

where  $\delta_2 = \delta_p - \delta_c$  and  $\delta_c = \omega_c - \omega_{32}$  are two-photon and control field detunings, respectively. From Eqs. (8) and (9), we iteratively solve the probe field coherence in perturbations of  $K_{\alpha\beta}$  with local field approximations [53] in Appendix B.

Along with the Maxwell-Bloch equation

$$\frac{d}{dz} \Omega_p = \frac{iD\Gamma}{2L} \tilde{\sigma}_{13}, \quad (10)$$

we obtain the EIT transmission  $T = |\Omega_p(L)/\Omega_p(z=0)|^2$  up to the  $M$ th order of perturbations as

$$T_M = \exp \left[ \frac{D\Gamma}{2} \text{Re} \left( \sum_{m=0}^M \frac{f_C^m}{A^{m+1}} \right) \right], \quad (11)$$

where we define the optical depth as  $D \equiv \rho \sigma L$  with an atomic density  $\rho$ , scattering cross section  $\sigma$ , and propagation length  $L$ . We further use the intrinsic decay rate  $\Gamma = 2\gamma_{31}$  as a universal measure with or without RDDI. The above, as  $M \rightarrow \infty$ , leads to

$$T = \exp \left[ \frac{D\Gamma}{2} \text{Re} \left( \frac{1}{A - f_C} \right) \right], \quad (12)$$

where

$$A \equiv i\delta_p - \gamma_{31} - \frac{i\Omega_c^2/4}{\delta_2 + i\gamma_{21}}, \quad (13)$$

$$f_C \equiv \frac{1}{N_z} \sum_{\alpha=1}^{N_z} \sum_{\beta \neq \alpha}^N K_{\alpha\beta}. \quad (14)$$

Equation (12) further indicates the effective collective frequency shift and linewidth,

$$\tilde{\delta}_p = \delta_p - \text{Im}[f_C], \quad \tilde{\gamma}_{31} = \gamma_{31} + \text{Re}[f_C], \quad (15)$$

respectively, where RDDIs directly modify the transparency condition and linewidth. We note that for singly excited collective states in  $N$  two-level atoms, we typically have  $N$  eigenmodes and associated eigenstates to fully describe the system dynamics [48,54]. It is the coherent forward scattering in the paraxial Maxwell-Bloch equation [46,48] that makes Eq. (15) a simple relation with a modification in frequency

shift and linewidth directly from the RDDI effect in the probe transition.

The transmission of Eq. (12) is valid only when  $|A| \gg |f_c|$ , which is easily satisfied since  $\Omega_c/|\delta_2 + i\gamma_{21}| \gg 1$  inside the transparency window or  $|A| \approx |\delta_p| \gg |f_c|$  when way off single-photon resonance. Near strong absorption in EIT spectrum, that is, at small transmission  $T$ , the iterative perturbations of  $K_{\alpha\beta}$  could fail since  $|A| \sim \gamma_{31}$ , which can be exceeded by  $|f_c|$ . However, for a large optical depth when  $D \gg |f_c|/\gamma_{31}$ , the transmission becomes vanishing, and therefore Eq. (12) still holds in this limit.

The clear advantage of EIT over fluorescence of two-level atoms in revealing the cooperative linewidth is manifested in the role of the control field. It is this large energy scale that validates infinite (all-order) perturbations of RDDI, and thus  $f_c$  can genuinely characterize the collective frequency shift and linewidth broadening of the probe photon. In contrast, in two-level atoms, multiple scattering of RDDI cannot be quantitatively calculated unless  $|f_c| \ll \gamma_{31}$ , which essentially shows no cooperative effect whatsoever. To get around this issue, a direct Monte Carlo simulation can be implemented to configure atomic spatial distributions, which leads to a coupling matrix involving RDDI. Numerically diagonalizing this coupling matrix between any two radiating dipoles effectively includes all-order scattering of RDDI [33,34]. However, this brute-force numerical method only applies well in a small Hilbert space, that is, of a small number of atoms (up to several thousands) with single-photon [33,34,54] or few-photon excitations [55]. A recently attempted numerical simulation tackled more than  $10^5$  atoms using an iterative method in calculating scattering rates [56] with repeated exact diagonalization of a subset of atoms. Therefore comparing several millions of atoms operated in fluorescence or even  $10^8$  atoms in EIT experiments, a huge gap nevertheless exists between theory and measurements [49], making direct comparison and prediction improbable in the near future.

It seems that modeling a much smaller number of atoms is feasible in our case, say,  $10^5$  atoms at most under the present computation capability. However, for the typical atomic density used in EIT experiments we consider here, a thousandfold decrease in the number of atoms (from  $10^8$  to  $10^5$ ) means a reduction of the optical depth to below 1 (from around 500 to 0.5) if the cross-sectional area of atoms, determined by a tightly focused probe field, is kept the same. This indicates a negligible RDDI effect on EIT properties up to  $N = 10^5$ . The parameter regime in most EIT experiments resides in the category of moderate atomic density with high optical depth and therefore large number of atoms as well, and this poses a dilemma in direct numerical simulations of the regime we consider here. To reveal the RDDI effect in a small sample numerically, one can consider an even higher density of atoms, where, however, the Maxwell-Bloch equations and Beer-Lambert law in this regime break down [49], and it is beyond the scope of our consideration in this paper. Meanwhile, EIT properties in a small sample with a high atomic density remain an open question and deserve future exploration.

We note that there has been a recent effort to apply the concept of the renormalization group method [57] to reduce the complexity of large system under strong RDDI into an ensemble of inhomogeneously broadened and weakly interacting

atoms. This is the essence of cooperativity in light-matter interactions, where many-atom physics could not be easily and simply extracted from a few-atom case. This complexity even augments when nonlocal RDDI is engaged in the dissipation process, where atom-atom correlations are certain to play important roles [41–43] in fluorescence measurements.

### III. LINEWIDTH OF PROBE LIGHT

We proceed to give an estimate of the effective linewidth  $f_c$  in Eq. (12) resulting from RDDI in a  $\Lambda$ -type EIT scheme.  $f_c$  is defined in Eq. (14) in the form of a discrete sum, where  $\sum_{\beta \neq \alpha}^N K_{\alpha\beta}$  can be treated with a referenced atom at position  $\mathbf{r}_\alpha$ . We will prove later that the leading-order result does not involve where  $\mathbf{r}_\alpha$  is, and therefore the  $N_z$  cross-grained average can just be replaced by the result of a single referenced atom.

We first calculate the part of the cooperative linewidth  $F_{\alpha\beta}$  in  $f_c$ , and the associated frequency shift can be derived accordingly from the cooperative linewidth. The continuous form of  $\tilde{\gamma}_{31} = \sum_{\beta=1}^N F_{\alpha\beta} e^{-i\mathbf{k}_p \cdot \mathbf{r}_{\alpha\beta}}/2$  including the intrinsic decay rate  $\gamma_{31}$  when  $\beta = \alpha$  becomes [30,58,59]

$$\tilde{\gamma}_{31} = N\gamma_{31} \int_{-\infty}^{\infty} dx dy dz (\pi^{3/2} R_{\perp}^{-2} R_L^{-1}) e^{-\frac{x^2+y^2}{R_{\perp}^2}} e^{-\frac{z^2}{R_L^2}} \times \int \frac{3}{8\pi} \left(1 - \frac{\sin^2 \theta}{2}\right) d\Omega_{\mathbf{k}} e^{-i\mathbf{k}_p \cdot (\mathbf{r}_\alpha - \mathbf{r})} e^{i\mathbf{k} \cdot (\mathbf{r}_\alpha - \mathbf{r})}, \quad (16)$$

where we have assumed Gaussian distributions with  $R_{\perp}$  and  $R_L$  for the transverse and longitudinal (propagation) length scales, respectively. The  $4\pi$  solid angle integration  $d\Omega_{\mathbf{k}}$  in the above comes from the original integral form of  $F_{\alpha\beta}$  [30], where circular polarizations are assumed and  $|\mathbf{k}| = |\mathbf{k}_p|$ . We further assume that  $\mathbf{r}_\alpha$  lies on the  $\hat{x}$ - $\hat{z}$  plane with an angle  $\theta'$  to  $\hat{z}$ , and we obtain

$$\tilde{\gamma}_{31} = \int \frac{3N\gamma_{31}}{8\pi} \left(1 - \frac{\sin^2 \theta}{2}\right) \sin \theta d\theta d\phi \times e^{-|\mathbf{k}_p|^2 R_{\perp}^2 \sin^2 \theta/4} e^{-|\mathbf{k}_p|^2 R_L^2 (1 - \cos \theta)^2/4} \times e^{i|\mathbf{k}_p||\mathbf{r}_\alpha|(\cos \theta \cos \theta' + \sin \theta \cos \phi \sin \theta' - \cos \theta')}. \quad (17)$$

We further integrate out the part of  $\int d\phi$ , which gives  $2\pi J_0(|\mathbf{k}_p||\mathbf{r}_\alpha| \sin \theta \sin \theta')$ , a Bessel function of the first kind. Since there are exponentially small weightings for  $\theta \sim \pi/2$  in the above Gaussian functions, we consider  $\theta \gtrsim 0$  and  $J_0(x') \approx 1 - x'^2/4$  for small  $x'$ . We then take its leading order and set  $x = \cos \theta$ , and we obtain

$$\tilde{\gamma}_{31} = \frac{3N\gamma_{31}}{8} \int_{-1}^1 (1 + x^2) dx e^{-\frac{|\mathbf{k}_p|^2 R_{\perp}^2 (1-x^2)}{4}} e^{-\frac{|\mathbf{k}_p|^2 R_L^2 (1-x)^2}{4}} \times e^{-i|\mathbf{k}_p||\mathbf{r}_\alpha| \cos \theta' (1-x)}. \quad (18)$$

When  $R_{\perp} = R_L$  and with  $|\mathbf{k}_p|R_L \gg 1$ , we can further simplify the above to

$$\tilde{\gamma}_{31} = \frac{3N\gamma_{31}}{8} \frac{2}{|\mathbf{k}_p|^2 R_L^2/2 + i|\mathbf{k}_p||\mathbf{r}_\alpha| \cos \theta'} \quad (19)$$

$$\approx \frac{3N\gamma_{31}}{2|\mathbf{k}_p|^2 R_L^2}. \quad (20)$$

Expressing the above in terms of an effective  $D_c = 2\rho\sigma R_L$  with  $\sigma = 3\lambda^2/(4\pi)$  and using the total volume  $V = \pi^{3/2}R_L^3$  of Gaussian density distributions and the averaged density  $\rho = N/V$ , we have  $\tilde{\gamma}_{31}/\gamma_{31} = \sqrt{\pi}D_c/4$ . We note that Eq. (20) has the same dependence of sizes as in a spherical geometry with considering only long-range terms in RDDI [59].

In general for a cigar shape, let  $a = |\mathbf{k}_p|^2 R_\perp^2/4$ ,  $b = |\mathbf{k}_p|^2 R_L^2/4$ , and  $m \equiv b/a$ , and from Eq. (18) we obtain

$$\frac{\tilde{\gamma}_{31}}{\gamma_{31}} = \frac{3N}{8} \frac{1}{4a^{3/2}(m-1)^{5/2}} \left\{ e^{\frac{a}{m-1}} \sqrt{\pi} (4am^2 - 4ma + m - 1 + 2a) \left[ \text{Erf}\left(\frac{(2m-1)\sqrt{a}}{\sqrt{m-1}}\right) - \text{Erf}\left(\frac{\sqrt{a}}{\sqrt{m-1}}\right) \right] + 2\sqrt{a}\sqrt{m-1}(e^{-4ma} - 2m + 1) \right\}, \quad (21)$$

where Erf is the error function. We note that the above expression provides a general recipe to describe the collective decay constant in a cigar shape of atoms with Gaussian distributions, which are relevant for realistic EIT experiments on long samples of atoms [9]. In the extreme needlelike shape where  $ma \gg 1$  and  $m \gg 1$ , we can further have the simple form

$$\tilde{\gamma}_{31}/\gamma_{31} = \frac{3N}{8} \frac{\sqrt{\pi}4am^2}{4a^{3/2}m^{5/2}} \times \frac{1}{2} = \frac{3\sqrt{\pi}}{8} \frac{N}{|\mathbf{k}_p|R_L}, \quad (22)$$

which shows the same dependence of the size in the long axis as in a uniform distribution of a needlelike geometry [58]. Again by using the total volume  $V = \pi^{3/2}R_\perp^2 R_L$  of Gaussian density distributions and the averaged density  $\rho = N/V$ , we derive the cooperative linewidth as

$$\tilde{\gamma}_{31}/\gamma_{31} = \frac{3\sqrt{\pi}}{8} \frac{N}{|\mathbf{k}_p|R_L} = \frac{\pi}{8} D_c \frac{|\mathbf{k}_p|R_\perp^2}{2R_L}, \quad (23)$$

where  $D_c = 2\rho\sigma R_L$  is the effective optical depth. We note that the relevant parameters  $\rho$ , optical depth  $D_c$ , total number of atoms  $N$ ,  $R_\perp$ , and  $R_L$  deterministically characterize the cooperative phenomena and enable a direct connection with EIT transmission measurements. These parameters are not independent of each other, since  $\rho = N/V$  with  $V = \pi^{3/2}R_\perp^2 R_L$  and optical depth  $D_c = 2\rho\sigma R_L$ .

In Fig. 2, we demonstrate the  $\tilde{\gamma}_{31}$  of Eq. (21) for three different  $R_\perp$ . For a fixed  $\rho$ ,  $\tilde{\gamma}_{31}$  is saturated as  $D_c$  increases for a small  $\rho$ , while it approaches a linear dependence for a larger  $\rho$ . For a smaller  $R_\perp$ ,  $\tilde{\gamma}_{31}$  appears less significant due to the small  $N$  or  $V$  involved for the cooperative linewidth at the same  $D_c$ . The interplay between  $R_\perp$  and  $\rho$  can be hardly distinguished in  $\tilde{\gamma}_{31}$ , which we show in the upper bounds of Fig. 2, where the case of  $\rho = 1-5 \times 10^{11} \text{ cm}^{-3}$  with a larger  $R_\perp$  almost overlaps with the case of  $\rho = 5 \times 10^{11} \text{ cm}^{-3}$  with a halved  $R_\perp$ . We also show almost identical lower bounds, as an example, for the cases of low  $\rho$  and smaller  $R_\perp$  in Fig. 2. This reflects the difficulty in determining precise atomic configurations of  $N$ ,  $\rho$ , or  $D_c$  straightforwardly from the cooperative linewidth  $\tilde{\gamma}_{31}$ , and therefore other complementary and independent measurements are necessary to ensure that these crucial parameters are relevant to the linewidth of the probe field. As for an extreme needlelike geometry, we find a suppressed  $\tilde{\gamma}_{31}$  due to the factor of  $|\mathbf{k}_p|R_\perp^2/R_L$ .

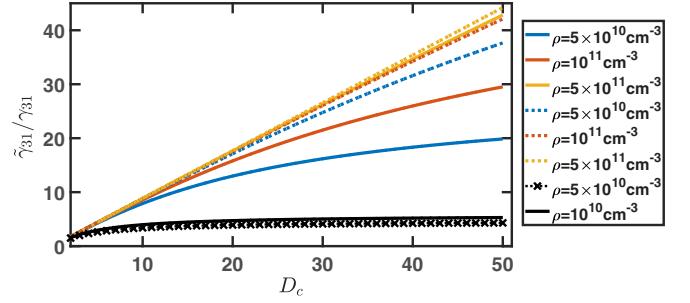


FIG. 2. Linewidth broadening from RDDI. We plot the enhanced decay rates  $\tilde{\gamma}_{31}$  normalized by an intrinsic decay constant  $\gamma_{31}$  for various atomic densities with  $R_\perp = 50$  (dashed curves), 25 (solid curves), and  $10 \mu\text{m}$  (curve with crosses). At a relatively low atomic density,  $\tilde{\gamma}_{31}$  is gradually saturated as  $D_c$  increases, while at a large density, it approaches a linear dependence on  $D_c$ . For a larger  $R_\perp$ , the linewidth broadens more significantly.

We note that if  $\rho$  and  $N$  are fixed (so is  $V$ ), increasing  $R_\perp$  would decrease the line broadening as there would be fewer atoms contributing to the enhanced decay rate along the propagation direction. This can be seen if we take  $\rho = 5 \times 10^{10} \text{ cm}^{-3}$  as an example, as shown in Fig. 2. As  $R_\perp$  increases from 25 to 50  $\mu\text{m}$ ,  $D_c = 50$  decreases to 12.5 for the same  $\rho$ ,  $N$ , and  $V$ . The corresponding  $\tilde{\gamma}_{31}$  in Fig. 2 reduces from 20 to 12.

The cooperative frequency shift [60,61] is related to the cooperative spontaneous decay rate, fulfilling Kramers-Kronig relations in electric susceptibility. We introduce an infrared cutoff of wave vector  $k_m = 2\pi/\sqrt[3]{V}$  in calculating the cooperative frequency shift [61], and we have

$$\delta_p = \delta_p - \frac{2}{\sqrt{\pi}} (\tilde{\gamma}_{31} - \gamma_{31}) \frac{\lambda}{\sqrt[3]{R_\perp^2 R_L}}, \quad (24)$$

with the probe field transition wavelength  $\lambda$ . For  $R_\perp = 50 \mu\text{m}$  and  $R_L = 1 \text{ mm}$ , we estimate a cooperative frequency shift of  $\sim \tilde{\gamma}_{31}/154.2$  for the moderate atomic density we consider in Fig. 2, which has less effect than the cooperative linewidth does in EIT spectroscopy.

#### IV. MULTIPLE SCATTERING OF RDDI IN TRANSMISSION

Next we directly apply the results of  $\tilde{\gamma}_{31}$  in the previous section from a general cigar-shaped geometry to the transmission property we obtained in Sec. II. Specifically, we compare the transmission property  $T$  of Eq. (12) under all-order scattering of RDDI to the one under a finite  $M$ th-order multiple-scattering effect in Eq. (11). With this comparison shown in Fig. 3, we are able to present the convergence of multiple scattering of RDDI and uncover the parameter regions in EIT spectroscopy where our perturbative treatment is most valid.

We first plot  $T$  of Eq. (12) in Fig. 3(a). As  $\tilde{\gamma}_{31}$  increases, the transmission window allows for shorter probe frequency spreads and thus puts more restrictions on light propagation and reduces storage efficiency. Larger cooperative linewidth also broadens the absorption peaks. We have absorbed the cooperative frequency shifts into  $\delta_p$ , which nonetheless can

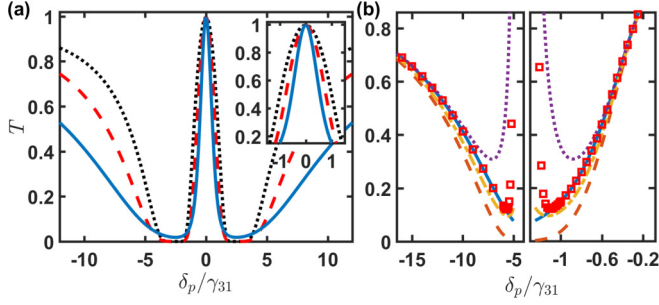


FIG. 3. EIT transmission and convergence of multiple scattering of RDDI. (a) The transmission  $T$  near two-photon resonance (inset) has shorter probe spreads from  $\tilde{\gamma}_{31}/\gamma_{31} = 1$  (dotted curve), to 2 (dashed curve), to 5 (solid curve), with  $D_c = 20$ ,  $\delta_c = 0$ ,  $\Omega_c = 5\gamma_{31}$ , and  $\gamma_{21}/\gamma_{31} = 0.001$ . The absorption peaks become broader at  $|\delta_p| \gtrsim \Omega_c$  as  $\tilde{\gamma}_{31}$  increases. (b) For the case of  $\tilde{\gamma}_{31}/\gamma_{31} = 5$  (solid curve), the multiple scattering of RDDI in  $T_M$  shows convergence inside the transparency window and at off resonance in the right and left panels, respectively, with scattering orders  $M = 1$  (dashed curve), 2 (dash-dotted curve), 3 (dotted curve), and 20 (squares).

also be observable in conventional EIT experiments. Next, in Fig. 3(b), we further compare the transmission with finite orders of multiple scattering of RDDI in Eq. (11). A clear convergence emerges toward a higher order of perturbations, both near transparency and in the off-resonance regimes. This demonstrates that our result of transmission  $T$  from Eq. (12) essentially involves all-order scattering of RDDI, which therefore enables a direct comparison with present experiments. Meanwhile, close to the transmission valley (absorption peaks), a divergence shows up, and the perturbation fails in this region of the EIT spectrum.

Finally, in Fig. 4 we plot the full width at half maximum (FWHM) of the transparency window as a dependence on the cooperative linewidth  $\tilde{\gamma}_{31}$  for various optical depths  $D_c$ . As the optical depth increases, this bandwidth decreases, as expected since in the limit of large  $\Omega_c$  but  $\Omega_c \ll \sqrt{D_c}\Gamma$ , it becomes [62,63]

$$\text{FWHM} = \sqrt{\frac{\ln(2)}{2}} \frac{\Omega_c^2}{\sqrt{D_c}\Gamma\tilde{\gamma}_{31}}, \quad (25)$$

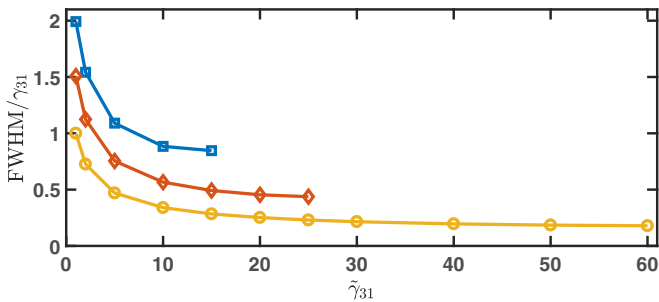


FIG. 4. FWHM of the EIT transmission window. We plot the FWHM of the transparency window for  $D_c = 20$  (squares), 40 (diamonds), and 100 (circles), for various cooperative linewidth broadenings  $\tilde{\gamma}_{31}$ . Other parameters of the EIT setup are the same as in Fig. 3.

which can be fitted by a Gaussian function of the detuning  $\delta_p$ . In contrast, for a finite  $\Omega_c$ , as the cooperative linewidth increases, the bandwidth decreases but is saturated for large  $D_c$ . In Fig. 4, we stop the bandwidth calculations at a certain  $D_c$  where Eq. (12) no longer genuinely determines the FWHM of the transparency regions. Furthermore, we find a scaling of  $\tilde{\gamma}_{31}^{-a}$  with  $a = 0.34, 0.41$ , and  $0.45$  for  $D_c = 20, 40$ , and  $100$ , respectively. This presents a significant reduction of the FWHM of the EIT transmission window in a more optically thick atomic ensemble.

In contrast, for a Rydberg EIT experiment [12] and theory [64], the transparency is suppressed due to Rydberg dipole-dipole interactions. This nonlinear interaction results in an effective photon-photon interaction, which can be applied in realizing photonic quantum gates and forming many-body photonic bound states. On the other hand, in EIT with RDDI here, the transparency does not change significantly since no photon-photon interaction is present. What is significantly modified is the transparency bandwidth, which is narrowed due to the finite cooperative linewidth. Moreover, the off-resonance absorption peaks are broadened, which can, along with the information of decreasing transparency bandwidth, further characterize the cooperative effect of RDDI in EIT.

## V. BEYOND THE LOCAL FIELD APPROXIMATION

Here, in the last section of our main results, we release the local field approximation, where multiple nonlocal scattering events of RDDI can be envisaged in EIT. In practical experiments for a large optical depth,  $K_{\alpha\beta}$  can be of the order of  $\gamma_{31}$ , and such that a perturbative treatment of  $K_{\alpha\beta}$  is only valid when RDDI is weak in a cold gas with a low density or near the transparency regions in the EIT scheme. We go beyond this approximation and proceed from Eqs. (A9) and (A11). We reevaluate the steady-state solutions still under the condition of a weak  $\Omega_p$ , and so we keep only the first order of  $\Omega_p$  in the Maxwell-Bloch equations of Eq. (A9).

For the first extension, we include the transverse part of the field dynamics; we will see later that it is necessary when RDDI becomes significant. Equation (A9) becomes

$$\left(-\frac{i}{2k_p}\nabla_{\perp}^2 + \frac{\partial}{\partial z}\right)\Omega_p(\mathbf{r}) = \frac{iD\Gamma}{2L}\tilde{\sigma}_{13}(\mathbf{r}), \quad (26)$$

where  $\nabla_{\perp}^2$  denotes the vector Laplacian in the transverse directions of  $\hat{x}$  and  $\hat{y}$ . The above presents a three-dimensional propagation equation (note that we use  $\mathbf{r}$  for the field and the dipole operator) with transverse dynamics, which takes care of refraction if there is strong RDDI.

The second extension goes to Eq. (A11), where we release the cross-section average and obtain

$$0 = \left[i\delta_p - \gamma_{31} - \frac{i|\Omega_c|^2}{4(\delta_2 + i\gamma_{21})}\right]\tilde{\sigma}_{13}^{\alpha} + i\frac{\Omega_p(\mathbf{r}_{\alpha})}{2} - \sum_{\beta \neq \alpha}^N K_{\alpha\beta}\tilde{\sigma}_{13}^{\beta}, \quad (27)$$

where we have substituted Eq. (B1). From the above, we further obtain, in discrete forms in space,

$$i\hat{M}\bar{\sigma}_{13} = -\frac{\bar{\Omega}_p}{2}, \quad (28)$$

$$\bar{\sigma}_{13} = \frac{i}{2}\hat{M}^{-1}\bar{\Omega}_p, \quad (29)$$

where  $\bar{\sigma}_{13} = [\sigma_{13}(r_1), \sigma_{13}(r_2), \dots, \sigma_{13}(r_N)]$ ,  $\bar{\Omega}_p = [\Omega_p(r_1), \Omega_p(r_2), \dots, \Omega_p(r_N)]$ , and

$$M = \begin{bmatrix} -A & K_{1,2} & K_{1,3} & \dots & K_{1,N} \\ K_{2,1} & -A & K_{2,3} & \dots & K_{2,N} \\ K_{3,1} & K_{3,2} & -A & \dots & \vdots \\ \vdots & \vdots & \vdots & \ddots & K_{N-1,N} \\ K_{N,1} & \dots & \dots & K_{N,N-1} & -A \end{bmatrix}, \quad (30)$$

with  $A = i\delta_p - \gamma_{31} - i|\Omega_c|^2/[4(\delta_2 + i\gamma_{21})]$ , which is also defined in Sec. II. From  $\hat{M}$ , we can see that the dipole operators are induced by or emerge from coupling to nonlocal fields.

Equations (26) and (29) together describe the propagation dynamics of a probe field with the effect of RDDI. By combining Eqs. (26) and (29) in the continuous limit, we obtain

$$\left(-\frac{i}{2k_p}\nabla_{\perp}^2 + \frac{\partial}{\partial z}\right)\Omega_p(\mathbf{r}) = -\frac{D\Gamma}{4L}\int\hat{M}^{-1}(\mathbf{r}-\mathbf{r}')\times\Omega_p(\mathbf{r}')\rho(\mathbf{r}')d\mathbf{r}', \quad (31)$$

where  $\rho(\mathbf{r})$  is the atomic density. The above results show that the probe field dynamics can be influenced by RDDI in both longitudinal and transverse directions. It reduces to conventional EIT in the single-particle picture when  $K_{\alpha,\beta} \rightarrow 0$ , leading to a local field propagation equation dominated simply by an electric susceptibility  $\chi \propto A^{-1}$ .

From Eq. (31), we note that a local field approximation we apply in perturbative treatments is valid only when the field is near the transparency or nonresonant regimes, that is, when the probe field  $\Omega_p(\mathbf{r})$  at arbitrary positions  $\mathbf{r}$  is not significantly attenuated and almost sustains its incident waveform at  $\mathbf{r} = 0$ , i.e.,  $\Omega_p(\mathbf{r}) \approx \Omega_p(\mathbf{r} = 0)$ . Under this condition, the effect of RDDI on the effective decay rate of the probe transition is most significant, since the integral in Eq. (31) goes through all the atoms. On the other hand, when the probe field is strongly attenuated, according to Eq. (31), no significant RDDI manifests in modifying the probe field dynamics. Therefore, to determine the full EIT spectrum and associated linewidth of the EIT window, a single quantity of the effective decay rate is not sufficient owing to this asymmetry of regimes, especially for an atomic gas with a high optical density.

We can formally solve Eq. (31) using Laplace transforms since it has convolution forms between the probe field and  $\hat{M}^{-1}$ . We then obtain (first neglecting the refraction terms and assuming a homogeneous gas  $\rho = N/V$ )

$$s\bar{\Omega}_p(s) - \Omega_p(z=0) = -\frac{D\Gamma}{4L}(N/L)\bar{M}^{-1}(s)\bar{\Omega}_p(s), \quad (32)$$

where  $F(s) \equiv \int_0^{\infty} f(r)e^{-sr}dr$  and  $s$  represents a complex number as for complex momentum spaces in Laplace trans-

forms of real spatial spaces  $r$  and  $r'$ . This further gives

$$\bar{\Omega}_p(s) = \frac{\Omega_p(z=0)}{s + \frac{D\Gamma}{4L}(N/L)\bar{M}^{-1}(s)}, \quad (33)$$

which can be inverse transformed in the complex plane back to  $\Omega_p(z=L)$  by

$$\Omega_p(z=L) = \frac{1}{2\pi i}\oint_{r-iR}^{r+iR}\bar{\Omega}_p(s)e^{sL}ds. \quad (34)$$

To further solve the above  $\Omega_p(z=L)$ , we assume again a perturbative RDDI, such that

$$M^{-1} = (-A\hat{I} + \hat{K})^{-1} \approx \frac{-1}{A}\left(\hat{I} + \frac{\hat{K}}{A}\right), \quad (35)$$

where  $\hat{K}$  represents the off-diagonal elements in Eq. (30). Now a weak RDDI can be approximated by a far-field expression in  $K(r-r') \rightarrow (3\Gamma/2)(-ie^{i\xi}e^{-ik_p\cdot(r-r')})/\xi$ . We finally obtain

$$\frac{\Omega_p(z=L)}{\Omega_p(z=0)} = \frac{1}{2\pi i}\oint\frac{e^{sL}ds}{s - \frac{D\Gamma}{4AL} - \frac{D\Gamma}{4AL}\left(\frac{N}{k_p L}\right)\left(\frac{3\Gamma/2}{A}\right)e^{as}\bar{\Gamma}(0, as)}, \quad (36)$$

where  $a$  is introduced in the Laplace transform of  $1/(|r-r'|+a)$  to remove the divergence when  $r \rightarrow r'$  and is in units of space as a complex length scale to renormalize the RDDI at divergence, and  $\bar{\Gamma}$  is an incomplete gamma function. The above is a square root of transmission, and the second term in the denominator of Eq. (36) is exactly the residue of the complex integral, leading to the EIT transmission  $[T = |\Omega_p(z=L)/\Omega_p(z=0)|^2]$  without RDDI,

$$\ln\left(\frac{\Omega_p(z=L)}{\Omega_p(z=0)}\right) = \frac{D\Gamma}{4A}.$$

Interestingly, the third term in the denominator of Eq. (36) shows the RDDI effect leading to multiple residues in the complex plane, which indicates the failure of expressing the EIT spectrum in terms of a single effective decay rate. We note that these multiple scales in decay constants show up even for the weak RDDI we consider here. In general, the multiple contributions of collective resonances and decay constants are most evident in low-dimensional and dense atomic arrays, and the field propagating through constituent particles cannot be genuinely described by a typical Beer-Lambert law [49] or Maxwell-Bloch equation in a macroscopic medium.

## VI. DISCUSSION AND CONCLUSION

Generally speaking, RDDIs are universal in all light-matter interacting systems, which are most prominent in a dense medium. They are responsible for many intriguing phenomena of super-radiance and subradiance and can be exploited to significantly enhance the performance of quantum storage efficiency in EIT under some tailored collective states [65]. Both these cooperative spontaneous emissions emerge from strong RDDIs, where multiple scattering of light exchanges between these quantum emitters dominates the dissipation process of the excited atoms.

This universal effect of RDDI should be observable as well in EIT media, but a systematic and evidence-based study

on the collective effect from RDDI has not been reported yet or fully accounted for in most of the theoretical investigations. We note that there are two central assumptions in our theory: weak field excitation and the local field approximation. The first assumption gives us the lowest level of hierarchy in the coupled equations, which also is associated with the first-order cumulant expansion we apply in this paper and ignorance of higher-order atom-atom correlations that would be relevant in dense media. The second assumption allows us to obtain the analytical forms of the RDDI effect on EIT properties, without which resolving the RDDI effect would otherwise require the full eigenspectrum of the system. We think it is the local field approximation that leads to a dramatic RDDI effect in our theoretical treatments, where the contributions of RDDI throughout the whole atomic ensemble are included at the local field. Therefore our predicted RDDI effect here could be overestimated compared with modern EIT experiments. Furthermore, we elaborate that a further advanced but computationally exhaustive quantum Langevin approach may provide a way to get around our assumptions here and take full account of light propagation, system dynamics, and atom-atom correlations in the large- $N$  limit.

For highly efficient EIT-based quantum memory applications [9,66,67], the atomic system is often prepared to be elongated along the propagation direction, leading to a high optical depth for the probe light. In these high-optical-density experiments, there is no clear observation of the RDDI effect on EIT spectroscopy, except that in Ref. [9] a mild dependence of the optical depth on the cooperative linewidth is conjectured in determining the experimental parameters by fitting EIT spectra and slow light traces. The fitted decay rate for the probe field transition has been shown to be enhanced two to three times as the optical density increases, which suggests the cooperative effect of RDDI in EIT. As a comparison with our predictions in Fig. 3, we have  $\tilde{\gamma}_{31}/\gamma_{31} \sim 27$  and 4.5 for  $R_{\perp} = 25$  and  $10 \mu\text{m}$ , respectively, at  $\rho = 5 \times 10^{10} \text{ cm}^{-3}$  with  $D_c = 400$ . This shows the overestimation of our model and quite a deviated range of predicted collective decay rates owing to different geometries of the atoms.

To clearly identify the RDDI effect with genuine comparisons, a further systematic investigation is needed to (i) accurately determine the number of atoms and the associated interacting volume along with its optical density and (ii) acquire a weak enough or single-photon source to serve as a probe field excitation. This way, our theory here can provide a direct comparison with EIT experiments to potentially unravel the effect of the RDDI on the line narrowing of the transmission window. It seems that the mild optical depth and standard atomic density in our theoretical consideration in Figs. 3 and 4 already suggest a clear signature of RDDI. We attribute this clear signature to our perturbative treatments using the local field approximation. A complexity can arise when this approximation is released as we have demonstrated in Sec. V, where multiple collective resonances and decay rates may participate in determining EIT transmission. We also note that the role of atom-atom correlations from RDDI can be crucial in light scattering of dense atoms [42,56], and they should as well be non-negligible in the large- $N$  and high-optical-depth sys-

tem we consider here. To include this effect of light-induced atom-atom correlations which are not accounted for in our theoretical treatment, either the next-order cumulants can be included or a quantum Langevin equation in positive- $P$  phase space [52,68,69] can be used to go beyond our perturbative treatments here.

As for Langevin equations on spontaneous emissions [26], quantum fluctuations or quantum noises play a role in initiating the dissipations of the excited atoms. In EIT, since the probe field intensity is under the normal order of field operators, it is commonly believed that the quantum fluctuations do not play a role in the probe field transmission [3,4]. We note here that one of the crucial assumptions in previous theoretical methods is the weak probe field approximation. Under this perturbation of the probe fields, up to single atomic excitation is allowed, and the collective spin excitation can form and lead to the popular picture of the dark-state polariton. This picture sustains the bosonic commutation relations of the quasiparticles in the large- $N$  limit and can explain some essential features of quantum storage and retrieval of single-photon propagation in EIT media. We emphasize that this assumption can be easily broken when the light-matter interacting system goes beyond the single-excitation limit when multiple excitations are present. When we have  $M$  atomic excitations in the atomic ensemble with  $M \lesssim N$ , naturally we face an exponential growth in the number of states in the dynamical Hilbert space of the order of  $C_M^N \sim O(N^M)$  if  $M \ll N$ . This indicates a dilemma and challenge we would encounter in any quantum systems when the full capacity of light-matter interactions is considered in describing their system dynamics.

A relevant platform which deviates from the conventional EIT setup and has distinct EIT properties is the Rydberg EIT scheme [11–14,70,71]. In this platform, which utilizes the high-lying Rydberg excited states, significant nonlinear effects of nonlocal dipole-dipole interactions emerge and reduce the performance of the probe field transparency. This interaction leads to the dipole blockade that forbids Rydberg excitations within the blockade radius, along with a significant energy shift away from the conventional transparency condition of two-photon resonance. Here, instead, we investigate the RDDI effect in the conventional EIT setup, where the dipole-dipole interactions are induced from the light exchanges between the atomic levels of the ground and the first excited states, even though RDDIs by nature have the feature of nonlocal interaction, similar to the Rydberg EIT scheme. By contrast, the dipole-dipole interactions in Rydberg EIT media directly result from the Rydberg excited levels. The theory of Rydberg EIT takes the strategy of a single-particle picture with a mean-field average of the Rydberg interactions, which results in an effective nonlocal and nonlinear interaction in the EIT spectrum. Two recent studies also present a demand for a more complete understanding of the Rydberg EIT system [72,73], where radiation trapping of scattered photons [72] or emerging nontrivial photon correlations [73] might be crucial to fill the gap between the mean-field models and experiments.

In conclusion, we have theoretically investigated the role of RDDI in EIT properties. We have predicted the effective cooperative linewidth and frequency shift in EIT

transmission from the multiple scattering of RDDI, which provides a direct comparison with experiment on the cooperative phenomena in EIT. The allowed transparent probe spread in the EIT transmission window is reduced due to a finite cooperative linewidth, which makes light storage less efficient in EIT-based quantum memory application. The phenomenon of RDDI in EIT should be observable in conventional EIT experiments in atoms with a moderate atomic density and optical depth. Finally, we note that our work here is just a starting point of the study of RDDI in EIT. The discrepancy

between the theory and experiment is noted and certainly deserves further exploration.

### ACKNOWLEDGMENTS

This work is supported by the Ministry of Science and Technology (MOST), Taiwan, under Grant No. MOST-109-2112-M-001-035-MY3. We are also grateful for support from Thematic Groups 1.2 and 3.2 of National Center for Theoretical Sciences in Taiwan.

### APPENDIX A: MAXWELL-BLOCH EQUATIONS FOR EIT WITH RDDI

In this Appendix, we derive the equations of motion for EIT with cooperative effects in the probe transition. We first define the slow-varying coherence operators as

$$\tilde{\sigma}_{13}(z, t) = \frac{1}{N_z} \sum_{\beta=1}^{N_z} \hat{\sigma}_{13}^{\beta}(z, t) e^{i\omega_p t - i\mathbf{k}_p \cdot \mathbf{r}_{\beta}}, \quad (\text{A1})$$

$$\tilde{\sigma}_{23}(z, t) = \frac{1}{N_z} \sum_{\beta=1}^{N_z} \hat{\sigma}_{23}^{\beta}(z, t) e^{i\omega_c t - i\mathbf{k}_c \cdot \mathbf{r}_{\beta}}, \quad (\text{A2})$$

$$\tilde{\sigma}_{12}(z, t) = \frac{1}{N_z} \sum_{\beta=1}^{N_z} \hat{\sigma}_{12}^{\beta}(z, t) e^{i\Delta\omega t - i\Delta\mathbf{k} \cdot \mathbf{r}_{\beta}}, \quad (\text{A3})$$

where  $\Delta\mathbf{k} = \mathbf{k}_p - \mathbf{k}_c$  and  $\Delta\omega = c|\Delta\mathbf{k}|$ . The same cross-section average is applied for the population operators,

$$\tilde{\sigma}_{11} = \frac{1}{N_z} \sum_{\beta=1}^{N_z} \hat{\sigma}_{11}^{\beta}(z, t), \quad \tilde{\sigma}_{22} = \frac{1}{N_z} \sum_{\beta=1}^{N_z} \hat{\sigma}_{22}^{\beta}(z, t), \quad \tilde{\sigma}_{33} = \frac{1}{N_z} \sum_{\beta=1}^{N_z} \hat{\sigma}_{33}^{\beta}(z, t).$$

These cross-grained averages of the slow-varying variables are typical treatments in solving the propagating quantized electric fields through an atomic medium. Later, for predictions of EIT properties, we shall not encounter the effect from cross-grained details, which is true since we take  $N$  and  $N_z \rightarrow \infty$ . In the following, we will consider only one-body atomic operators in the dynamically light-matter coupled equations, which truncates the hierarchy of the equations and equivalently neglects small higher-order multiatom correlations.

In the copropagating frame  $\tau = t - z/c$ , we obtain the Maxwell-Bloch equations as

$$\frac{d}{d\tau} \tilde{\sigma}_{23} = (i\delta_c - \gamma_{21} - \gamma_{32}) \tilde{\sigma}_{23} + i \frac{\Omega_c}{2} (\tilde{\sigma}_{22} - \tilde{\sigma}_{33}) + i \frac{\Omega_p}{2} \tilde{\sigma}_{12}^{\dagger}, \quad (\text{A4})$$

$$\frac{d}{d\tau} \tilde{\sigma}_{13} = (i\delta_p - \gamma_{31}) \tilde{\sigma}_{13} + i \frac{\Omega_c}{2} \tilde{\sigma}_{12} + i \frac{\Omega_p}{2} (\tilde{\sigma}_{11} - \tilde{\sigma}_{33}) - \frac{1}{N_z} \sum_{\alpha=1}^{N_z} \sum_{\beta \neq \alpha}^N K_{\alpha\beta} (\tilde{\sigma}_{11}^{\alpha} - \tilde{\sigma}_{33}^{\alpha}) \tilde{\sigma}_{13}^{\beta}, \quad (\text{A5})$$

$$\frac{d}{d\tau} \tilde{\sigma}_{12} = (i\delta_2 - \gamma_{21}) \tilde{\sigma}_{12} - i \frac{\Omega_p}{2} \tilde{\sigma}_{23}^{\dagger} + i \frac{\Omega_c^*}{2} \tilde{\sigma}_{13}, \quad (\text{A6})$$

$$\frac{d}{d\tau} \tilde{\sigma}_{11} = 2\gamma_{31} \tilde{\sigma}_{33} + 2\gamma_{21} \tilde{\sigma}_{22} - i \frac{\Omega_p}{2} \tilde{\sigma}_{13}^{\dagger} + i \frac{\Omega_p^*}{2} \tilde{\sigma}_{13} + \frac{1}{N_z} \sum_{\alpha=1}^{N_z} \sum_{\beta \neq \alpha}^N [K_{\alpha\beta} (\tilde{\sigma}_{31}^{\alpha} \tilde{\sigma}_{13}^{\beta}) + K_{\alpha\beta}^* (\tilde{\sigma}_{31}^{\beta} \tilde{\sigma}_{13}^{\alpha})], \quad (\text{A7})$$

$$\frac{d}{d\tau} \tilde{\sigma}_{33} = -\gamma_3 \tilde{\sigma}_{33} + i \frac{\Omega_p}{2} \tilde{\sigma}_{13}^{\dagger} - i \frac{\Omega_p^*}{2} \tilde{\sigma}_{13} + i \frac{\Omega_c}{2} \tilde{\sigma}_{23}^{\dagger} - i \frac{\Omega_c^*}{2} \tilde{\sigma}_{23} - \frac{1}{N_z} \sum_{\alpha=1}^{N_z} \sum_{\beta \neq \alpha}^N [K_{\alpha\beta} (\tilde{\sigma}_{31}^{\alpha} \tilde{\sigma}_{13}^{\beta}) + K_{\alpha\beta}^* (\tilde{\sigma}_{31}^{\beta} \tilde{\sigma}_{13}^{\alpha})], \quad (\text{A8})$$

$$\frac{d}{dz} \Omega_p = \frac{iD\Gamma}{2L} \tilde{\sigma}_{13}, \quad (\text{A9})$$

where  $K_{\alpha\beta} \equiv (F_{\alpha\beta} + i2G_{\alpha\beta}) e^{-i\mathbf{k}_p \cdot \mathbf{r}_{\alpha\beta}} / 2$  [30]. The slow-varying atomic operators, not the cross-grained ones, are denoted as  $\tilde{\sigma}_{\mu\nu}^{\beta}$ , and, for example,  $\tilde{\sigma}_{13}^{\beta} = \hat{\sigma}_{13}^{\beta} e^{i\omega_p t - i\mathbf{k}_p \cdot \mathbf{r}_{\beta}}$ . The optical depth is  $D \equiv \rho\sigma L$ , and  $\gamma_3 = 2\gamma_{31} + 2\gamma_{32}$ . The two-photon detuning is  $\delta_2 = \delta_p - \delta_c$ . The RDDI in the

probe transition modifies the transition coherence  $\tilde{\sigma}_{13}$  and redistributes the populations of  $\tilde{\sigma}_{11}$  and  $\tilde{\sigma}_{33}$  through multiatom correlations.

In this  $\Lambda$ -type atomic system, we assume that all  $N$  atoms are initially prepared in  $|1\rangle$ . In the limit of a weak probe

field, which corresponds to a linear dependence of  $\Omega_p$  in the coupled equations, we have  $\tilde{\sigma}_{11} = 1$ ,  $\tilde{\sigma}_{22} = \tilde{\sigma}_{33} = 0$ , and  $\tilde{\sigma}_{23} = 0$ . The relevant equations for atomic coherences (with implicit spatial dependence of  $z$ ) are

$$\frac{d}{d\tau}\tilde{\sigma}_{12} \approx (i\delta_2 - \gamma_{21})\tilde{\sigma}_{12} + i\frac{\Omega_c^*}{2}\tilde{\sigma}_{13}, \quad (\text{A10})$$

$$\frac{d}{d\tau}\tilde{\sigma}_{13} \approx (i\delta_p - \gamma_{31})\tilde{\sigma}_{13} + i\frac{\Omega_c}{2}\tilde{\sigma}_{12} + i\frac{\Omega_p}{2} - \frac{1}{N_z} \sum_{\alpha=1}^{N_z} \sum_{\beta \neq \alpha}^N K_{\alpha\beta} \tilde{\sigma}_{13}^{\beta}. \quad (\text{A11})$$

## APPENDIX B: STEADY-STATE SOLUTIONS

Here, we proceed to find the steady-state solutions of the coupled equations in Appendix A and present how the effect of the RDDI modifies the EIT spectrum. The steady-state solution of the ground-state coherence from Eq. (A10) gives

$$\tilde{\sigma}_{12} = \frac{-\Omega_c^*/2}{\delta_2 + i\gamma_{21}}\tilde{\sigma}_{13}. \quad (\text{B1})$$

We then substitute  $\tilde{\sigma}_{12}$  from the above in Eq. (A11), and in the zeroth order of  $K_{\alpha\beta}$ , for a real constant  $\Omega_c$ , we derive the coherence of the probe transition (now retrieving the spatial dependence for clarity)

$$\tilde{\sigma}_{13}^{(0)}(z) = \frac{-i\Omega_p(z)/2}{i\delta_p - \gamma_{31} - \frac{i\Omega_c^2/4}{\delta_2 + i\gamma_{21}}} \equiv \frac{-i\Omega_p(z)/2}{A}, \quad (\text{B2})$$

which is proportional to the electric field susceptibility in conventional EIT theory without cooperative effects. We define  $A$  above for later concise representation of the cooperative effect on the linewidth of the EIT spectrum.

Next for the first-order perturbation of  $K_{\alpha\beta}$ , we apply the zeroth-order results of Eq. (B2) to Eq. (A11) and obtain

$$\tilde{\sigma}_{13}^{(1)}(z) = \frac{-i\Omega_p(z)/2}{A} + \frac{1}{AN_z} \sum_{\alpha=1}^{N_z} \sum_{\beta \neq \alpha}^N K_{\alpha\beta} \tilde{\sigma}_{13}^{\beta(0)}(\mathbf{r}_\beta), \quad (\text{B3})$$

where a coupling between the atomic coherences at  $z$  and other positions  $\mathbf{r}_\beta \neq \mathbf{r}_\alpha$  appears due to RDDI. Equation (B3) essentially describes nonlocal interactions of the fields. We proceed to apply the local field approximation to Eq. (B3) and obtain

$$\tilde{\sigma}_{13}^{(1)}(z) = \frac{-i\Omega_p(z)/2}{A} + \frac{f_C}{A} \frac{-i\Omega_p(z)/2}{A}, \quad (\text{B4})$$

where  $f_C = N_z^{-1} \sum_{\alpha=1}^{N_z} \sum_{\beta \neq \alpha}^N K_{\alpha\beta}$  denotes the cooperative dipole-dipole interactions between the cross-grained region and all the other atoms in the ensemble. We calculate the leading order of  $f_C$  in the main text, which is independent of the cross-grained region and is cooperatively enhanced due to the involvement of all  $N$  atoms of the medium.

From light propagation of Eq. (A9) in the Maxwell-Bloch equations, we replace the above  $\tilde{\sigma}_{13}$  with  $\tilde{\sigma}_{13}^{(1)}(z)$  of Eq. (B4), and  $\Omega_p(L)$  becomes

$$\ln\left(\frac{\Omega_p(L)}{\Omega_p(0)}\right) = \frac{D\Gamma}{4} \left(\frac{1}{A} + \frac{f_C}{A^2}\right) \approx \frac{D\Gamma}{4} \frac{1}{A - f_C}, \quad (\text{B5})$$

where the approximate form in the above is valid when  $|f_C| \ll |A|$ , and it suggests that there are effective  $\tilde{\delta}_p^{(1)}$  and  $\tilde{\gamma}_{31}^{(1)}$  in  $A$ , which are

$$\tilde{\delta}_p^{(1)} = \delta_p - \text{Im}[f_C], \quad \tilde{\gamma}_{31}^{(1)} = \gamma_{31} + \text{Re}[f_C]. \quad (\text{B6})$$

These represent a cooperative frequency shift in  $\delta_p$  and linewidth broadening (larger than  $\gamma_{31}$ ), respectively, and their superscripts denote the single scattering event of RDDI.

To account for the multiple-scattering effect in EIT theory, similar to the treatment of coherent scattering of two-level atoms [74–76], we obtain the steady-state solutions of Eq. (A11) by considering a second-order perturbation, which reads

$$0 = A\tilde{\sigma}_{13}^{(2)} + \frac{i\Omega_p}{2} - f_C\tilde{\sigma}_{13}^{(1)}. \quad (\text{B7})$$

From the above and using the result of  $\tilde{\sigma}_{13}^{(1)}$ , we have

$$\tilde{\sigma}_{13}^{(2)} = \frac{-i\Omega_p}{2} \left[ \frac{1}{A} + \frac{f_C}{A^2} + \frac{f_C^2}{A^3} \right]. \quad (\text{B8})$$

Again from Eq. (A9), we obtain the output field,

$$\ln\left(\frac{\Omega_p(L)}{\Omega_p(0)}\right) = \frac{D\Gamma}{4L} \int_0^L dz \left[ \frac{1}{A} + \frac{f_C}{A^2} + \frac{f_C^2}{A^3} \right], \quad (\text{B9})$$

$$\approx \frac{D\Gamma}{4} \frac{1}{A - f_C},$$

where the approximate form can be derived from the first line by using Taylor expansion,  $(1-x)^{-1} = \sum_{n=0}^{\infty} x^n$  for  $x < 1$ .

- 
- [1] S. E. Harris, J. E. Field, and A. Imamoglu, *Phys. Rev. Lett.* **64**, 1107 (1990).  
[2] S. E. Harris, *Phys. Today* **50**(7), 36 (1997).  
[3] M. D. Lukin, *Rev. Mod. Phys.* **75**, 457 (2003).  
[4] M. Fleischhauer, A. Imamoglu, and J. P. Marangos, *Rev. Mod. Phys.* **77**, 633 (2005).  
[5] K. Hammerer, A. S. Sørensen, and E. S. Polzik, *Rev. Mod. Phys.* **82**, 1041 (2010).  
[6] L. V. Hau, S. E. Harris, Z. Dutton, and C. H. Behroozi, *Nature (London)* **397**, 594 (1999).  
[7] U. Schnorrberger, J. D. Thompson, S. Trotzky, R. Pugatch, N. Davidson, S. Kuhr, and I. Bloch, *Phys. Rev. Lett.* **103**, 033003 (2009).  
[8] M. Fleischhauer and M. D. Lukin, *Phys. Rev. A* **65**, 022314 (2002).  
[9] Y.-F. Hsiao, P.-J. Tsai, H.-S. Chen, S.-X. Lin, C.-C. Hung, C.-H. Lee, Y.-H. Chen, Y.-F. Chen, I. A. Yu, and Y.-C. Chen, *Phys. Rev. Lett.* **120**, 183602 (2018).  
[10] Y. Wang, J. Li, S. Zhang, K. Su, Y. Zhou, K. Liao, S. Du, H. Yan, and S.-L. Zhu, *Nat. Photonics* **13**, 346 (2019).

- [11] M. Saffman, T. G. Waller, and K. Mølmer, *Rev. Mod. Phys.* **82**, 2313 (2010).
- [12] J. D. Pritchard, D. Maxwell, A. Gauguet, K. J. Weatherill, M. P. A. Jones, and C. S. Adams, *Phys. Rev. Lett.* **105**, 193603 (2010).
- [13] Y. O. Dudin and A. Kuzmich, *Science* **336**, 887 (2012).
- [14] T. Peyronel, O. Firstenberg, Q. Liang, S. Hofferberth, A. V. Gorshkov, T. Pohl, M. D. Lukin, and V. Vuletic, *Nature (London)* **488**, 57 (2012).
- [15] M. Mücke, E. Figueroa, J. Bochmann, C. Hahn, K. Murr, S. Ritter, C. J. Villas-Boas, and G. Rempe, *Nature (London)* **465**, 755 (2010).
- [16] T. Kampschulte, W. Alt, S. Manz, M. Martinez-Dorantes, R. Reimann, S. Yoon, D. Meschede, M. Bienert, and G. Morigi, *Phys. Rev. A* **89**, 033404 (2014).
- [17] R. Röhlsberger, H.-C. Wille, K. Schlage, and B. Sahoo, *Nature (London)* **482**, 199 (2012).
- [18] P. R. Hemmer, A. V. Turukhin, M. S. Shahriar, and J. A. Musser, *Opt. Lett.* **26**, 361 (2001).
- [19] V. M. Acosta, K. Jensen, C. Santori, D. Budker, and R. G. Beausoleil, *Phys. Rev. Lett.* **110**, 213605 (2013).
- [20] G. B. Serapiglia, E. Paspalakis, C. Sirtori, K. L. Vodopyanov, and C. C. Phillips, *Phys. Rev. Lett.* **84**, 1019 (2000).
- [21] B. S. Ham, P. R. Hemmer, and M. S. Shahriar, *Opt. Commun.* **144**, 227 (1997).
- [22] A. V. Turukhin, V. S. Sudarshanam, M. S. Shahriar, J. A. Musser, B. S. Ham, and P. R. Hemmer, *Phys. Rev. Lett.* **88**, 023602 (2001).
- [23] J. J. Longdell, E. Fraval, M. J. Sellars, and N. B. Manson, *Phys. Rev. Lett.* **95**, 063601 (2005).
- [24] E. Baldit, K. Bencheikh, P. Monnier, S. Briau, J. A. Levenson, V. Crozatier, I. Lorgeré, F. Bretenaker, J. L. Le Gouët, O. Guillot-Noël, and Ph. Goldner, *Phys. Rev. B* **81**, 144303 (2010).
- [25] G. Heinze, C. Hubrich, and T. Halfmann, *Phys. Rev. Lett.* **111**, 033601 (2013).
- [26] M. O. Scully and M. S. Zubairy, *Quantum Optics* (Cambridge University Press, Cambridge, 1997).
- [27] L. Jiang, H. Pu, W. Zhang, and H. Y. Ling, *Phys. Rev. A* **80**, 033606 (2009).
- [28] H. H. Jen and D.-W. Wang, *Phys. Rev. A* **87**, 061802(R) (2013).
- [29] H. H. Jen and D.-W. Wang, *J. Opt. Soc. Am. B* **31**, 2931 (2014).
- [30] R. H. Lehmburg, *Phys. Rev. A* **2**, 883 (1970).
- [31] R. H. Dicke, *Phys. Rev.* **93**, 99 (1954).
- [32] M. Gross and S. Haroche, *Phys. Rep.* **93**, 301 (1982).
- [33] S. L. Bromley, B. Zhu, M. Bishof, X. Zhang, T. Bothwell, J. Schachenmayer, T. L. Nicholson, R. Kaiser, S. F. Yelin, M. D. Lukin, A. M. Rey, and J. Ye, *Nat. Commun.* **7**, 11039 (2016).
- [34] W. Guerin, M. O. Araújo, and R. Kaiser, *Phys. Rev. Lett.* **116**, 083601 (2016).
- [35] Y. Sonnefraud, N. Verellen, H. Sobhani, G. A. E. Vandenbosch, V. V. Moshchalkov, P. V. Dorpe, P. Nordlander, and S. A. Maier, *ACS Nano* **4**, 1664 (2010).
- [36] B. H. McGuyer, M. McDonald, G. Z. Iwata, M. G. Tarallo, W. Skomorowski, R. Moszynski, and T. Zelevinsky, *Nat. Phys.* **11**, 32 (2015).
- [37] S. D. Jenkins, J. Ruostekoski, N. Pappas, S. Savo, and N. I. Zheludev, *Phys. Rev. Lett.* **119**, 053901 (2017).
- [38] R. Röhlsberger, K. Schlage, B. Sahoo, S. Couet, and R. Ruffer, *Science* **328**, 1248 (2010).
- [39] J. Keaveney, A. Sargsyan, U. Krohn, I. G. Hughes, D. Sarkisyan, and C. S. Adams, *Phys. Rev. Lett.* **108**, 173601 (2012).
- [40] Z. Meir, O. Schwartz, E. Shahmoon, D. Oron, and R. Ozeri, *Phys. Rev. Lett.* **113**, 193002 (2014).
- [41] J. Pellegrino, R. Bourgain, S. Jennewein, Y. R. P. Sortais, A. Browaeys, S. D. Jenkins, and J. Ruostekoski, *Phys. Rev. Lett.* **113**, 133602 (2014).
- [42] S. Jennewein, M. Besbes, N. J. Schilder, S. D. Jenkins, C. Sauvan, J. Ruostekoski, J.-J. Greffet, Y. R. P. Sortais, and A. Browaeys, *Phys. Rev. Lett.* **116**, 233601 (2016).
- [43] S. D. Jenkins, J. Ruostekoski, J. Javanainen, R. Bourgain, S. Jennewein, Y. R. P. Sortais, and A. Browaeys, *Phys. Rev. Lett.* **116**, 183601 (2016).
- [44] S. J. Roof, K. J. Kemp, M. D. Havey, and I. M. Sokolov, *Phys. Rev. Lett.* **117**, 073003 (2016).
- [45] M. H. Oliveira, C. E. Máximo, and C. J. Villas-Boas, *Phys. Rev. A* **104**, 063704 (2021).
- [46] S. Jennewein, L. Brossard, Y. R. P. Sortais, A. Browaeys, P. Cheinet, J. Robert, and P. Pillet, *Phys. Rev. A* **97**, 053816 (2018).
- [47] M. O. Araújo, I. Krešić, R. Kaiser, and W. Guerin, *Phys. Rev. Lett.* **117**, 073002 (2016).
- [48] R. T. Sutherland and F. Robicheaux, *Phys. Rev. A* **93**, 023407 (2016).
- [49] L. Chomaz, L. Corman, T. Yefsah, R. Desbuquois, and J. Dalibard, *New J. Phys.* **14**, 055001 (2012).
- [50] C. Cohen-Tannoudji, J. Dupont-Rock, and G. Grynberg, *Atom-Photon Interactions: Basic Processes and Applications* (Wiley, New York, 1992).
- [51] R. Kubo, *J. Phys. Soc. Jpn.* **17**, 1100 (1962).
- [52] P. D. Drummond and S. J. Carter, *J. Opt. Soc. Am. B* **4**, 1565 (1987).
- [53] S. Sevinçli, N. Henkel, C. Ates, and T. Pohl, *Phys. Rev. Lett.* **107**, 153001 (2011).
- [54] H. H. Jen, M.-S. Chang, and Y.-C. Chen, *Phys. Rev. A* **94**, 013803 (2016).
- [55] H. H. Jen, *Phys. Rev. A* **96**, 023814 (2017).
- [56] F. Robicheaux and R. T. Sutherland, *Phys. Rev. A* **101**, 013805 (2020).
- [57] F. Andreoli, M. J. Gullans, A. A. High, A. Browaeys, and D. E. Chang, *Phys. Rev. X* **11**, 011026 (2021).
- [58] N. E. Rehler and J. H. Eberly, *Phys. Rev. A* **3**, 1735 (1971).
- [59] I. E. Mazets and G. Kurizski, *J. Phys. B: At., Mol. Opt. Phys.* **40**, F105 (2007).
- [60] M. O. Scully, *Phys. Rev. Lett.* **102**, 143601 (2009).
- [61] H. H. Jen, *Ann. Phys. (Amsterdam)* **360**, 556 (2015).
- [62] M. D. Lukin, M. Fleischhauer, A. S. Zibrov, H. G. Robinson, V. L. Velichansky, L. Hollberg, and M. O. Scully, *Phys. Rev. Lett.* **79**, 2959 (1997).
- [63] Y.-C. Wei, B.-H. Wu, Y.-F. Hsiao, P.-J. Tsai, and Y.-C. Chen, *Phys. Rev. A* **102**, 063720 (2020).
- [64] D. Petrosyan, J. Otterbach, and M. Fleischhauer, *Phys. Rev. Lett.* **107**, 213601 (2011).
- [65] A. Asenjo-Garcia, M. Moreno-Cardoner, A. Albrecht, H. J. Kimble, and D. E. Chang, *Phys. Rev. X* **7**, 031024 (2017).

- [66] Y.-W. Cho, G. T. Campbell, J. L. Everett, J. Bernu, D. B. Higginbottom, M. T. Cao, J. Geng, N. P. Robins, P. K. Lam, and B. C. Buchler, *Optica* **3**, 100 (2016).
- [67] P. Vernaz-Gris, K. Huang, M. Cao, A. S. Sheremet, and J. Laurat, *Nat. Commun.* **9**, 363 (2018).
- [68] C. W. Gardiner and P. Zoller, *Quantum Noise: A Handbook of Markovian and Non-Markovian Quantum Stochastic Methods with Applications to Quantum Optics*, 2nd ed. (Springer-Verlag, Berlin, 2000).
- [69] H. H. Jen, *Phys. Rev. A* **85**, 013835 (2012).
- [70] S.-S. Hsiao, K.-T. Chen, and I. A. Yu, *Opt. Express* **28**, 28414 (2020).
- [71] B. Kim, K.-T. Chen, S.-S. Hsiao, S.-Y. Wang, K.-B. Li, J. Ruseckas, G. Juzeliūnas, T. Kirova, M. Auzinsh, Y.-C. Chen, Y.-F. Chen, and I. A. Yu, *Commun. Phys.* **4**, 101 (2021).
- [72] P. Bienias, J. Douglas, A. Paris-Mandoki, P. Titum, I. Mirgorodskiy, C. Tresp, E. Zeuthen, M. J. Gullans, M. Manzoni, S. Hofferberth, D. Chang, and A. V. Gorshkov, *Phys. Rev. Research* **2**, 033049 (2020).
- [73] A. Tebben, C. Hainaut, A. Salzinger, S. Geier, T. Franz, T. Pohl, M. Gärtner, G. Zürn, and M. Weidemüller, *Phys. Rev. A* **103**, 063710 (2021).
- [74] O. Morice, Y. Castin, and J. Dalibard, *Phys. Rev. A* **51**, 3896 (1995).
- [75] M.-T. Rouabah, M. Samoylova, R. Bachelard, P. W. Courteille, R. Kaiser, and N. Piovella, *J. Opt. Soc. Am. A* **31**, 1031 (2014).
- [76] L. Corman, J. L. Ville, R. Saint-Jalm, M. Aidelsburger, T. Bienaimé, S. Nascimbène, J. Dalibard, and J. Beugnon, *Phys. Rev. A* **96**, 053629 (2017).